Supplementary Information

FRET binding antenna reports spatiotemporal dynamics of GDI-Cdc42 GTPase interactions

[1,2]Louis Hodgson[%,*], [1]Désirée Spiering[%], [3]Mohsen Sabouri-Ghomi, [2]Onur Dagliyan, [4]Céline DerMardirossian, [3,5]Gaudenz Danuser*, [2]Klaus M. Hahn*

[1]Department of Anatomy and Structural Biology and Gruss-Lipper Biophotonics Center, Albert Einstein College of Medicine; [2]Department of Pharmacology and Lineberger Cancer Center, University of North Carolina at Chapel Hill; [3]Department of Cell Biology, The Scripps Research Institute; [4]Department of Immunology and Microbial Science, The Scripps Research Institute; [5]Department of Cell Biology, Harvard Medical School.

[%]authors contributed equally

*address correspondence to:

Louis Hodgson, louis.hodgson@einstein.yu.edu

Gaudenz Danuser, Gaudenz.Danuser@UTSouthwestern.edu

Klaus Hahn, khahn@med.unc.edu

Supplementary Results

Supplementary Figures

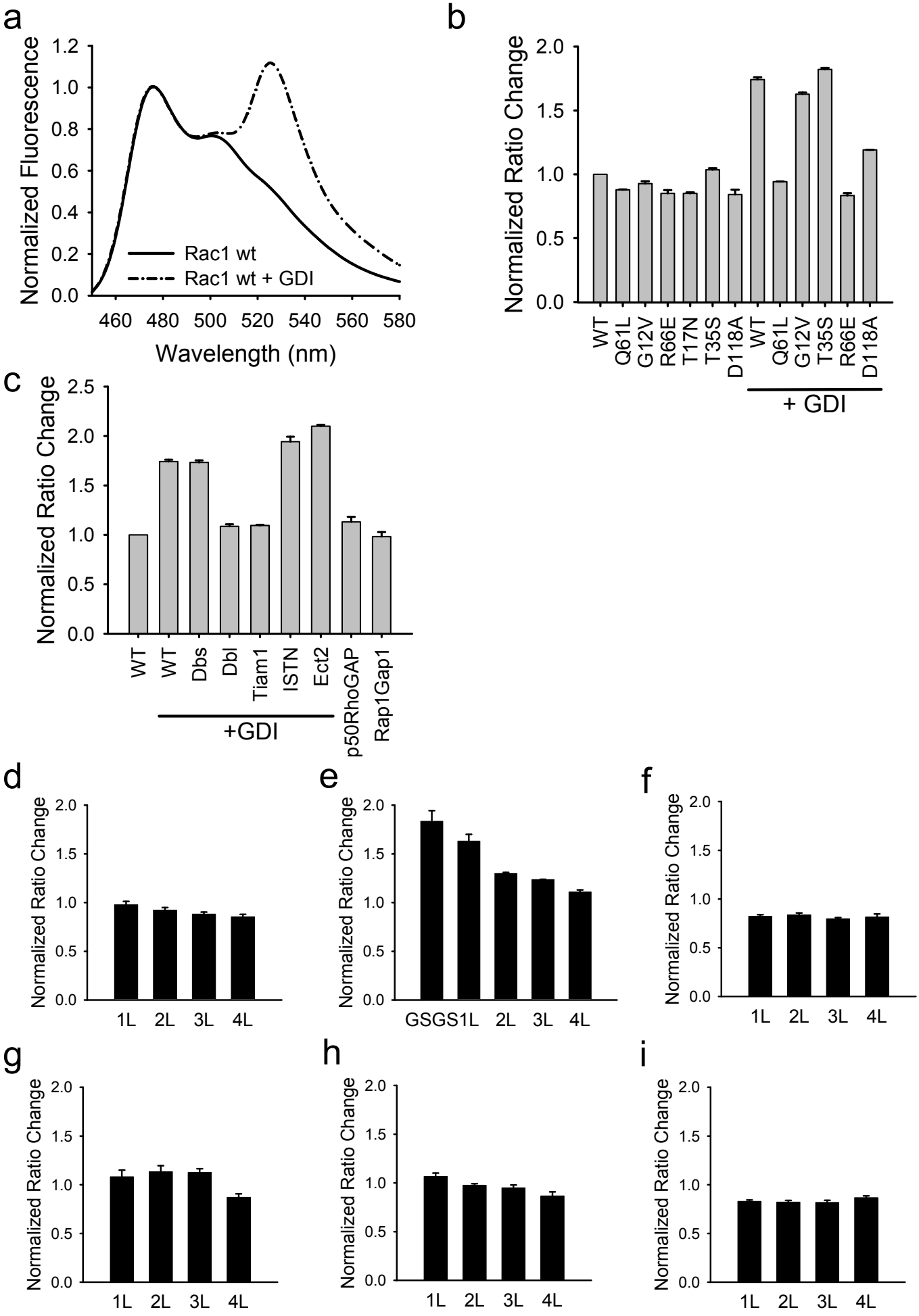

Supplementary Figure 1

Supplementary Fig. 1: Optimization and characterization of the GDI.Rac1 FLARE biosensor. a, Normalized emission spectra of GDI.Rac1 FLARE in HEK 293T cells (excitation 433 nm; normalized at 474 nm emission peak). Solid line, wild-type biosensor; dash-dotted line, excess co-expressed GDI. **b**, Normalized FRET/CFP emission ratios of GDI.Rac1 FLARE mutants, expressed with and without excess GDI. Results are the mean of three independent measurements. Error bars represent ±SEM. **c**, Normalized FRET/CFP emission ratios of wildtype GDI.Rac1 FLARE with co-expressed GEFs or GAPs (see legend to Fig. 1). Results are the mean of three independent measurements. Error bars represent ±SEM. **d-i,** Optimization of linkers and fluorescent proteins was first carried out on Rac1, and results of this used as a starting point for Cdc42.GDI FLARE optimization. The extent of change induced by GDI binding depended on the length of the linker between the mCerulean and Venus and on the circular permutant of Venus. Optimization of Rac1 was carried out with wild type Venus that includes residue A206. (**d**) shows wild type Venus and mCerulean, (**e**) shows Venus permuted such that the original residue 49 becomes the new N terminus. The other circular permutants had new N termini at the following original residues:, (**f**) 157, (**g**) 173, (**h**) 195, and (**i**) 229 [1]. The linker length between mCerulean and Venus was varied in repeating units ("1 – 4L") of 17 amino acids (TSGSGKPGSGEGSTKGG), optimized for flexibility, solubility and resistance to proteases [2]. In (**e**), an additional shorter linker comprising of "GSGS" was tested. Changes in FRET/mCer ratio with and without GDI are shown (GDI-bound/GDI-free). N=3 experiments, with ±SEM. Cp49Venus with the "GSGS" linker, (**e**) produced the best change in FRET ratio. These changes gave the optimal response used in the GDI.Cdc42 biosensor. For (**d**) **–** (**i**), results are the mean of three independent experiments. Error bars represent ±SEM.

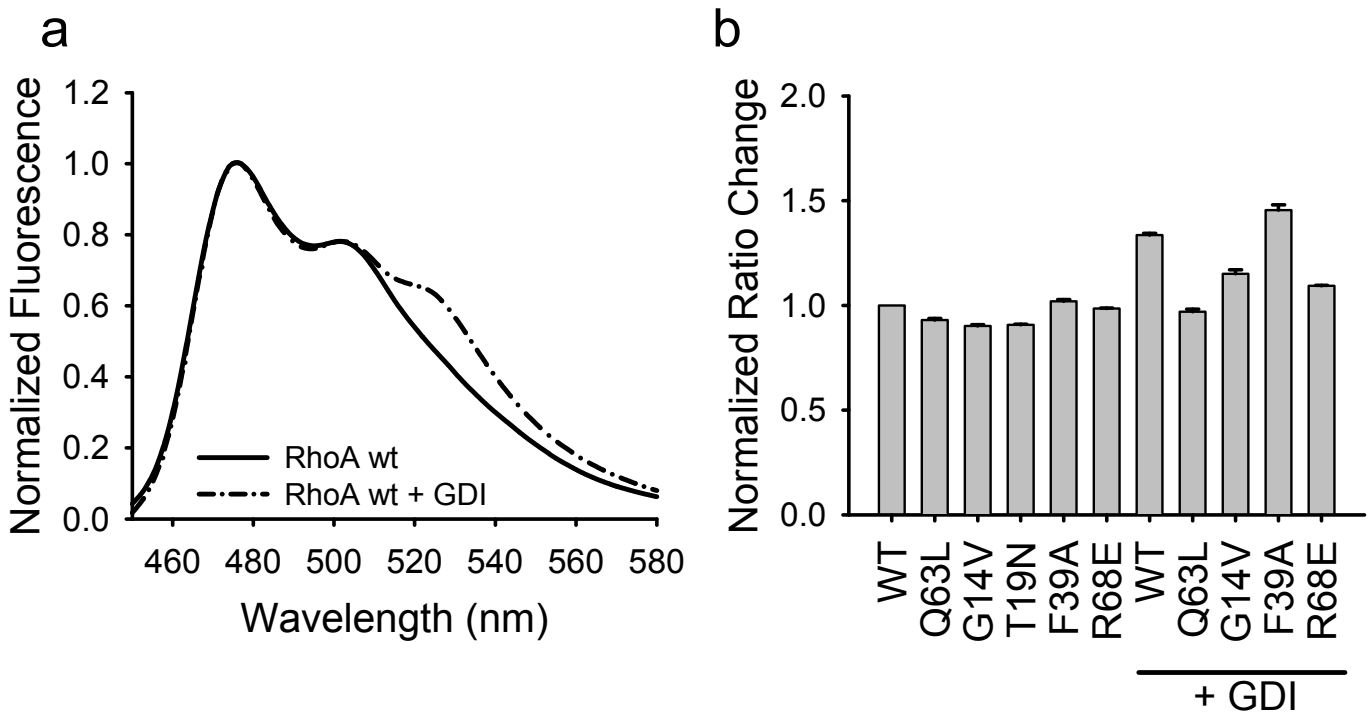

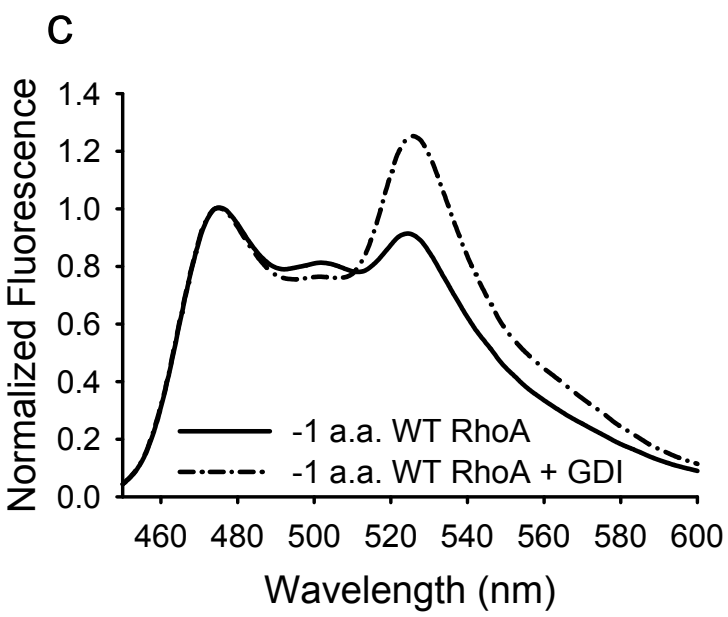

Supplementary Figure 2

Supplementary Fig. 2: GDI-RhoA biosensor. a, Representative, normalized emission spectra of GDI.RhoA FLARE in HEK 293T cells (excitation 433 nm; normalized at 474 nm emission peak). Solid line, wild-type biosensor; dash-dotted line, excess coexpressed GDI. **b**, Normalized FRET/CFP emission ratios of GDI.RhoA FLARE mutants, expressed with and without excess GDI. Results are the mean of three independent experiments. Error bars represent ±SEM. **c.** Linker optimization began using the configuration described in **Supplementary Figure 1**. Improved response was obtained by further removing 1 amino acid from the linker, the first methionine of RhoA; representative, normalized emission spectra of GDI.RhoA FLARE in HEK 293T cells (excitation 433 nm; normalized at 474 nm emission peak). Solid line, wild-type biosensor; dash-dotted line, excess co-expressed GDI.

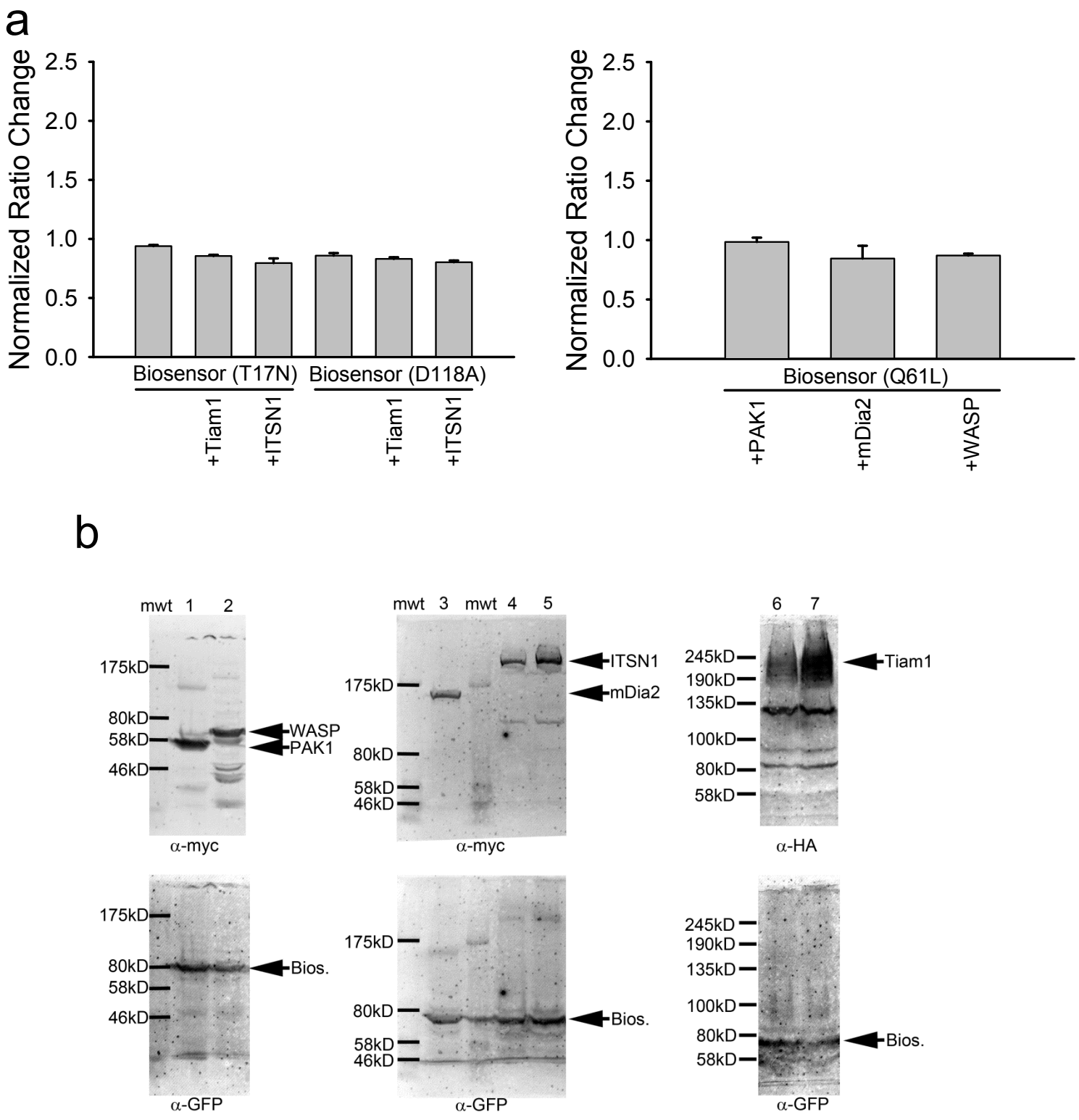

Supplementary Figure 3

Supplementary Fig. 3: a, Binding of full-length, Cdc42-interacting GEFs (**LEFT**) and effectors (**RIGHT**) does not result in GDI.Cdc42 FLARE biosensor FRET change. Full-length, wild-type Tiam1 and Intersectin1 (GEFs), and PAK1, mDia2, and WASP (effectors) were coexpressed in HEK 293T cells at 4x excess cDNA concentration together with the GDI.Cdc42.FLARE mutants T17N and D118A (mutant versions that bind to GEFs with high affinity) or Q61L (mutant version that bind to effectors with high affinity), respectively. Results are the mean of three independent measurements. Error bars represent ±SEM. **b**, Expressions of GEFs and effectors shown in (**a**) confirmed in HEK 293T cells. Lane 1: Q61L version of the biosensor with wildtype myc-PAK1 full length; lane 2: Q61L version of the biosensor with wildtype myc-WASP full length; lane 3: Q61L version of the biosensor with wildtype myc-mDia2 full length; lane 4: T17N version of the biosensor with wildtype myc-Intersectin1 full length; lane 5: D118A version of the biosensor with wildtype myc-Intersectin1 full length; lane 6: T17N version of the biosensor with wildtype HA-Tiam1 full length; and lane 7: D118A version of the biosensor with wildtype HA-Tiam1 full length. Expressions of the corresponding biosensors are shown below. Lanes 1 and 2 are in an 8% SDS-PAGE gel and lanes 3 – 7 are in a 6% SDS-PAGE gel.

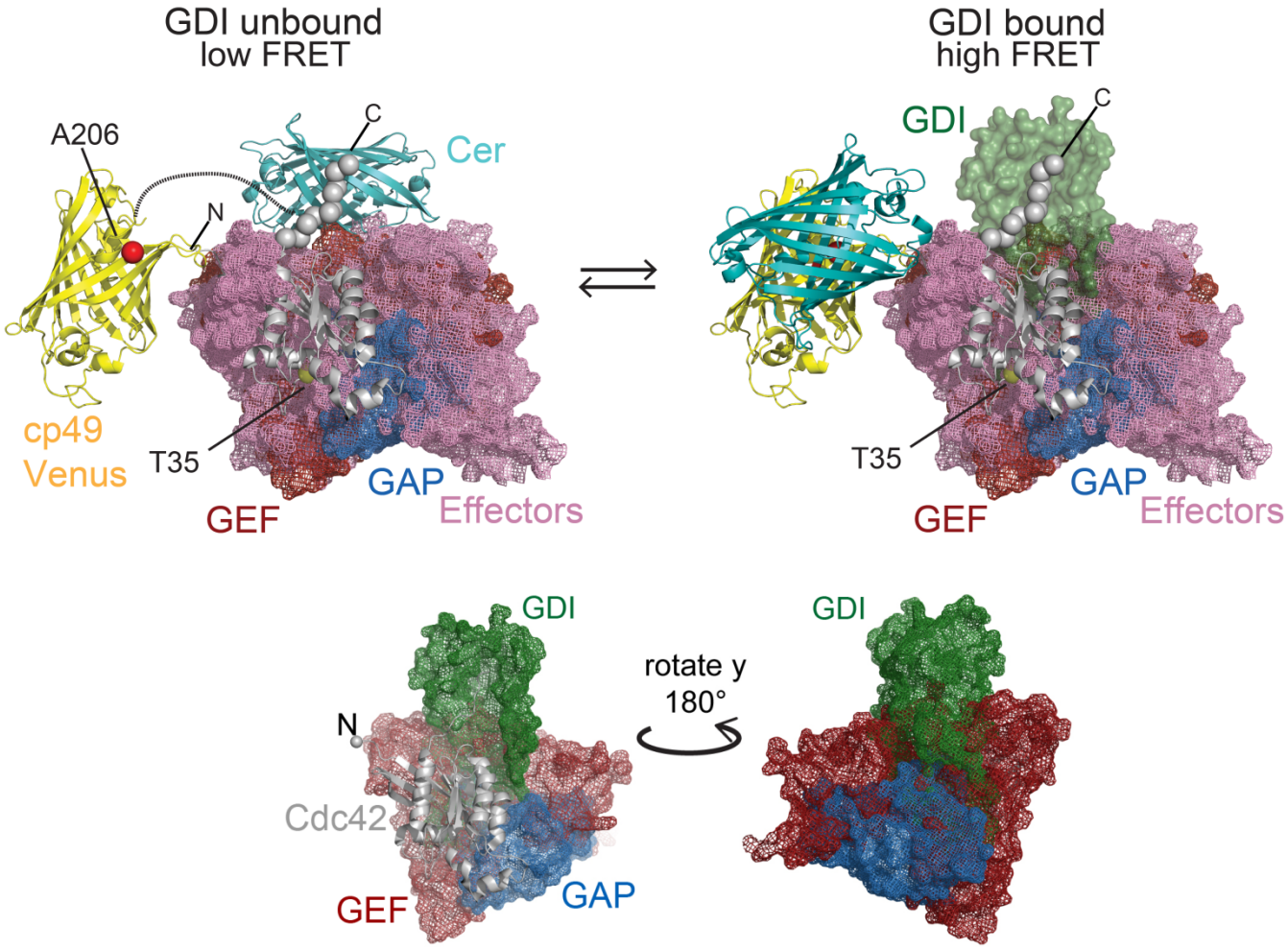

Supplementary Figure 4

Supplementary Fig. 4: The hypothetical structure of the GDI.Cdc42 FLARE biosensor. Interactions of the antenna-Cdc42 chimera with RhoGDI (green), Dbs (red), and Cdc42GAP (blue) were analyzed using crystal structures of protein complexes from the PDB. The FRET antenna (comprised of mCerulean and a specific circular permutant of Venus) was attached to the N-terminus of Cdc42**.** Possible GDI-free, low FRET and GDI-bound, high FRET configurations are shown (see text). In the model shown here, the mobility of Cer fluorescent protein is restricted in the absence of GDI because Cer interacts with Cdc42 regions that bind GDI, near the Cdc42 C terminus. Binding of GEFs or GAPs would not influence this interaction, as shown at the bottom. When GDI displaces the mCer, FRET is enhanced through the heterodimerization of the fluorescent proteins. An A206K mutation in cp49 Venus (red sphere), known to reduce heterodimerization, reduced FRET in the GDI-bound state. Alternate models are proposed in the text.

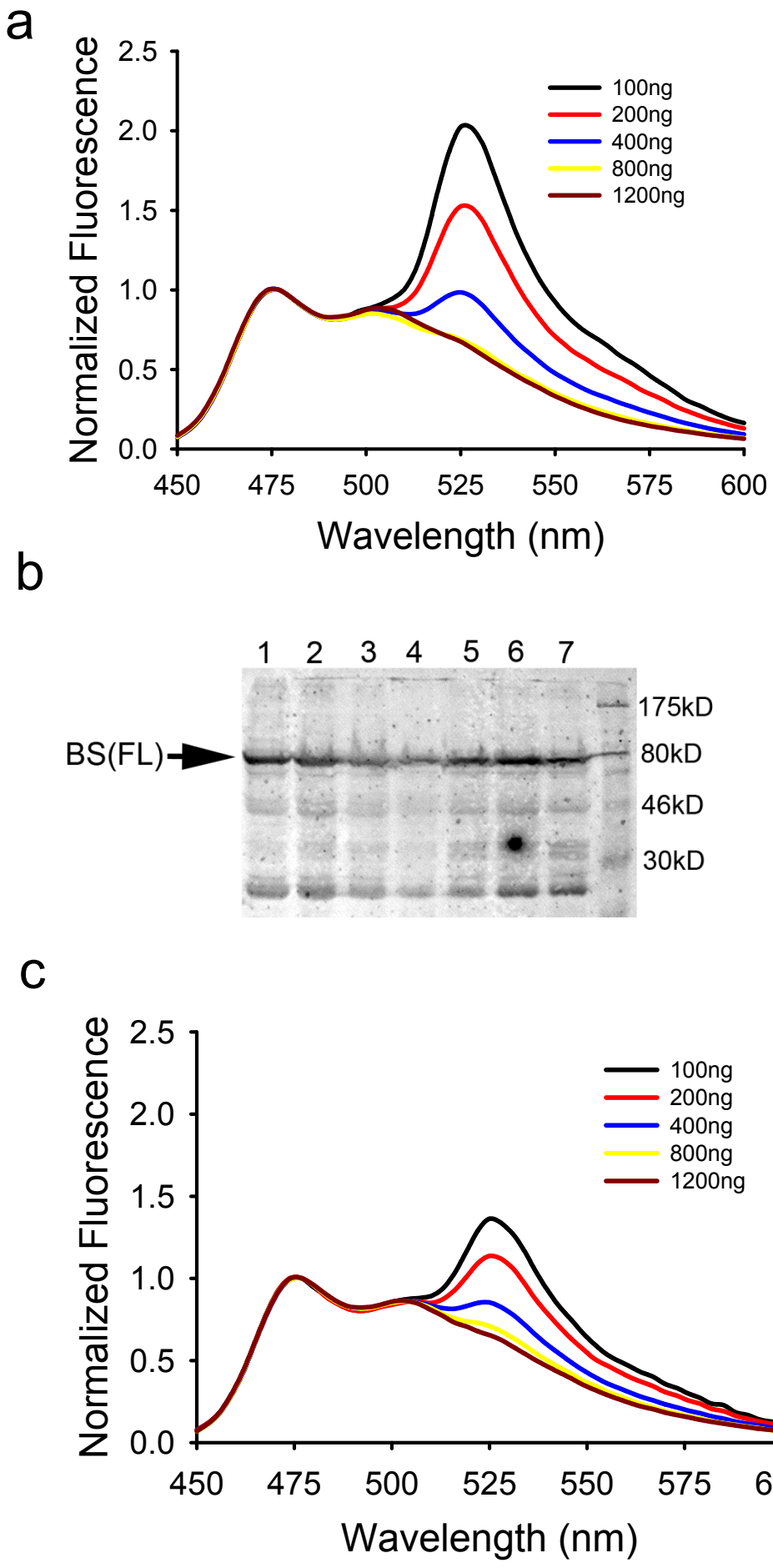

Supplementary Figure 5

Supplementary Fig. 5: Titration of normal and mutant GDI.Cdc42 FLARE biosensors against endogenous GDI in HEK 293T cells. Representative, normalized emission spectra of GDI.Cdc42 FLARE biosensors in HEK 293T cells (excitation 433 nm; normalized at 474 nm emission peak). **a,** The expression of the GDI.Cdc42 FLARE biosensor was titrated in HEK 293T cells. In this normal biosensor version, a fluorescent protein mutation that reduces fluorescent protein dimerization (A206K) [3] was used in the mCerulean but not in cpVenus. The legend indicates the amount of biosensor cDNA used during transfection. **b**, Full-length expression of the GDI.Cdc42 FLARE biosensor mutants confirmed in HEK 293T cells used for fluorometric biosensor validations. Lane 1: Wild-type; lane 2: T35S; lane 3: Q61L; lane 4: G12V; lane 5: T17N; lane 6: R66E; and lane 7: D118A. **c,** The GDI.Cdc42 FLARE biosensor was modified to include the monomerizing mutation (A206K) in both fluorescent proteins. Legend indicates the amount of the biosensor cDNA used during transfection.

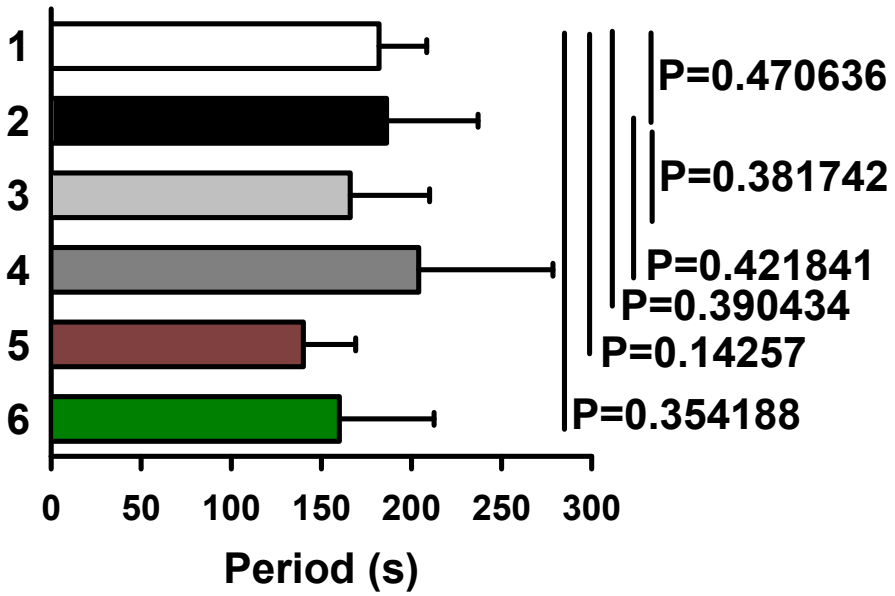

1: without biosensor
2: Cdc42 & GDI.Cdc42 FLARE (T35S) multiplexed
3: GDI.Cdc42 FLARE (wildtype)
4: Scrambled RNA control
5: Y156E KD/rescue
6: Y156F KD/rescue

Supplementary Figure 6

Supplementary Fig. 6: Periodicity of protrusion/retraction cycles measured from the autocorrelation functions of edge velocity. Periodicity was determined by taking the spline-fitted, 2000× bootstrap-averaged autocorrelation functions for each condition and measuring the time to the peak of the first side lobe after the zero-crossing. Averaged autocorrelation function for each condition was calculated from the following sample sizes: 1. n = 854 individual windows in 8 cells; 2. n = 420 individual windows in 7 cells; 3. n = 704 individual windows in 8 cells; 4. n = 1154 individual windows in 9 cells; 5. n = 979 individual windows in 11 cells; and 6. n = 902 individual windows in 11 cells. Student t-test was used to determine the p-values, as indicated, *<0.05.

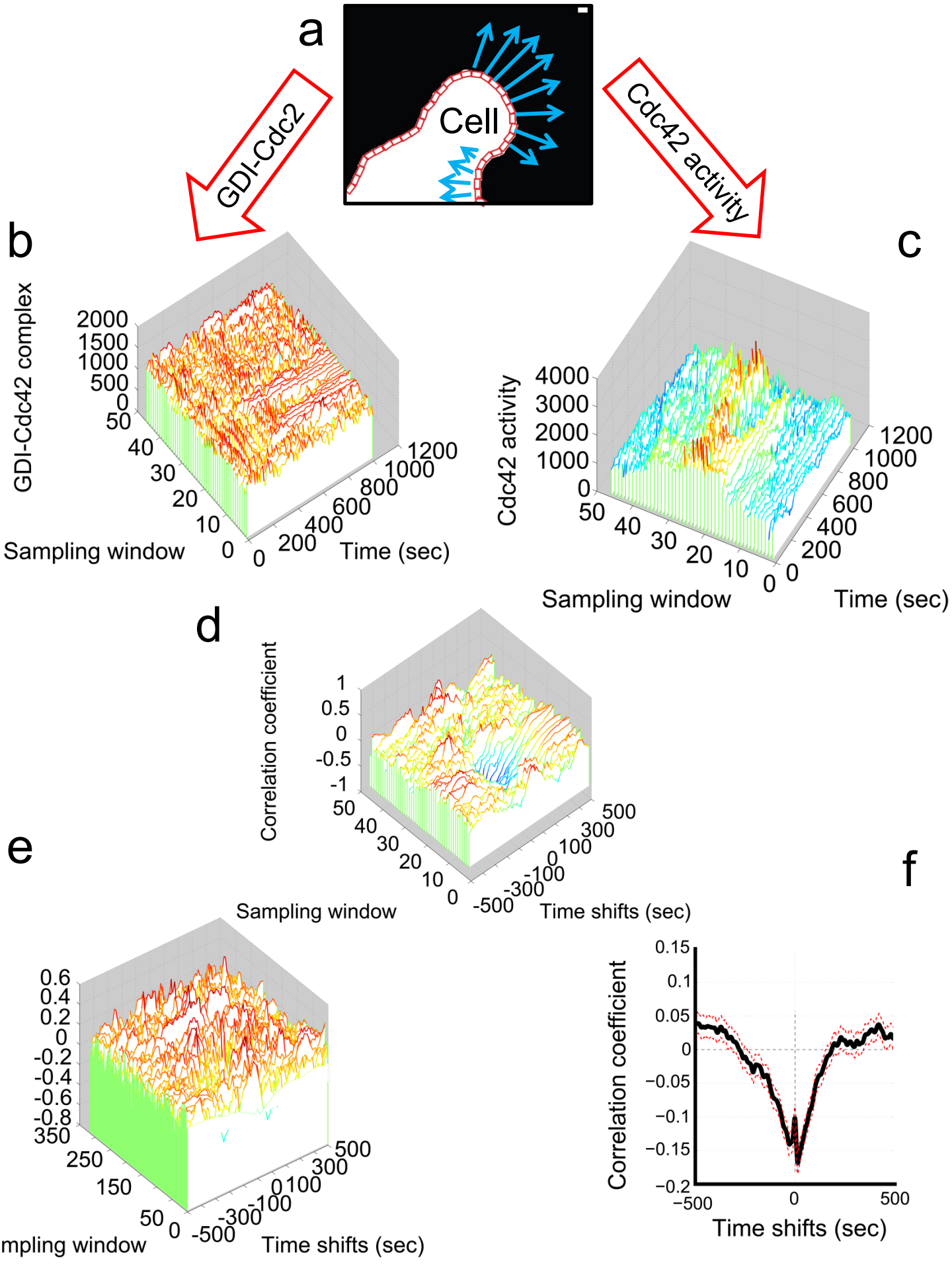

Supplementary Figure 7

Supplementary Fig. 7: Correlation analysis used in Figs 2 – 4 illustrated on an example of direct correlation between GDI-Cdc42 complex localization and Cdc42 activation. a, Biosensor signals are sampled in probing windows located at the cell edge (0 – 0.9 μm; as shown), or in parallel bands 0.9 – 1.8 μm, 1.8 – 2.7 μm or 2.7 – 3.6 μm from the edge. The initial window width is set to ~2 microns. As the windows move with the cell edge windows in protruding areas expand in width up to ~3 microns, whereas windows in retracting areas shrink in width. Each sampling window produces a time series of the imaged biosensor signal and associated local edge velocity (arrows) **b**, Time series of GDI-Cdc42 complex for all sampling windows activity along the edge. **c**, Time-series of Cdc42 activity for all sampling windows along the edge. **d**, Local coupling of GDI-Cdc42 complex and Cdc42 activity assessed by cross-correlation of the two time series in each sampling window. **e**, Global coupling is assessed by accumulating the local couplings over all sampling windows of a cell population. **f**, Average cross-correlation (black line) is computed from all correlations in individual windows. 95%-confidence interval (red dotted lines) is estimated by a non-parametric bootstrap of the difference between an overall fit of the correlation functions and a per-cell fit. Accordingly, these confidence bands reflect the uncertainty of the correlation due to cell-cell variation. Note that in this flow chart any of the two biosensor samplings can be replaced by an edge velocity sampling in order to generate correlation curves between the other biosensor and edge velocity.

a

b

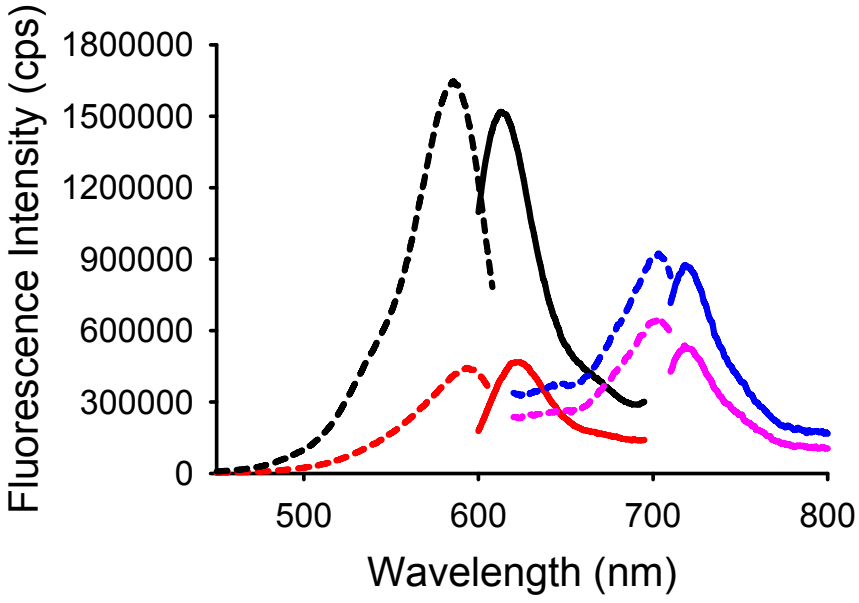

c

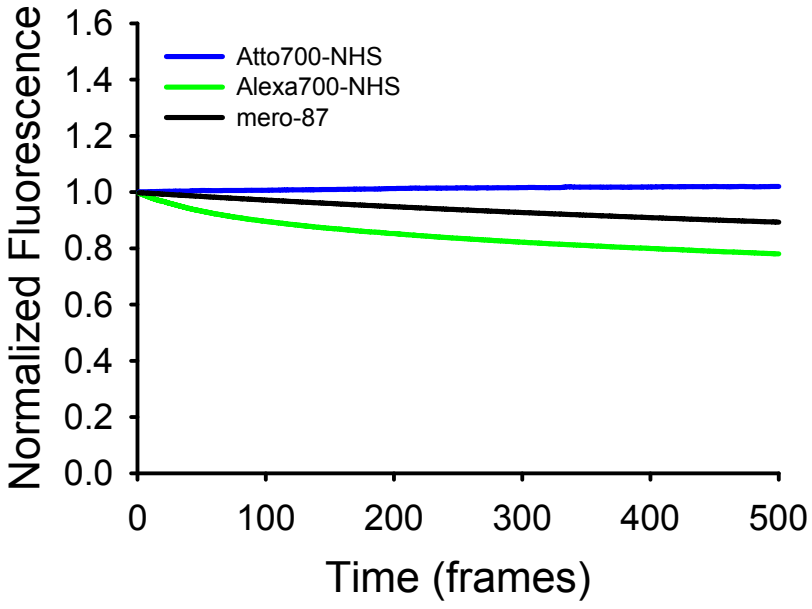

Supplementary Figure 8

Supplementary Fig. 8: Modification of the MeroCBD biosensor enabling use in the same cell as the GDI.Cdc42 FLARE biosensor. a, The environment-sensing dye mero87 was placed where it responds to Cdc42 binding, and the Atto-700 was added for ratio imaging. **b**, Excitation and emission spectra of the modified meroCBD in the presence of activated Cdc42 (GTPγS-loaded, black and blue) and of inactive Cdc42 (GDP-loaded, red and magenta). Atto-700 is at longer wavelengths. Dashed lines indicate excitation, solid lines indicate emission. **c**, Representative spectra showing the photostability of far red dyes used in the modified meroCBD biosensor. 100μM dye solutions were mounted on coverslips and imaged for the indicated duration using a 100W Hg lamp with a neutral density filter of 1.3 and exposure times of 1 sec/frame.

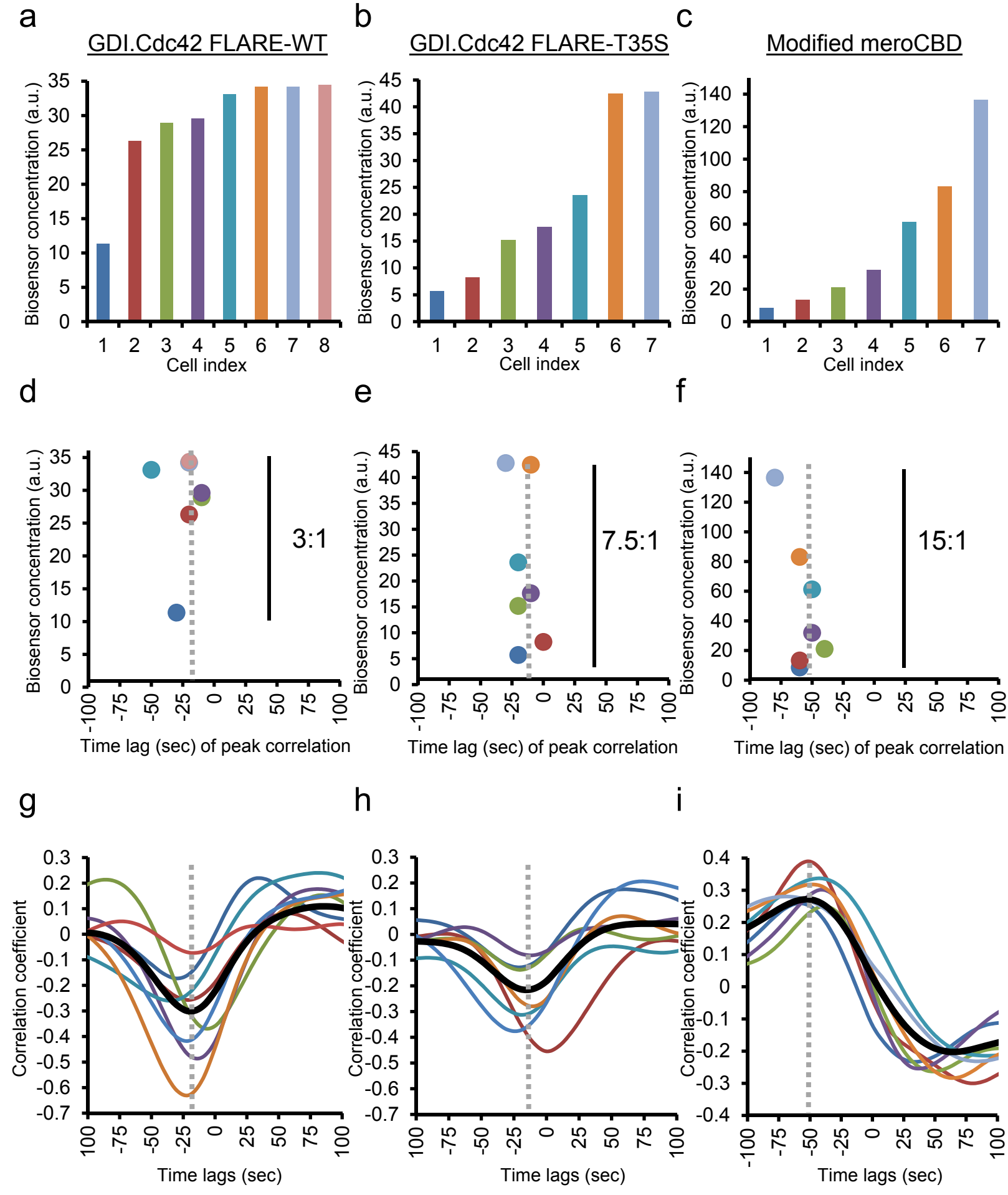

Supplementary Figure 9

Supplementary Fig. 9: Sensitivity of image measurements to GDI-Cdc42 biosensor concentration. We quantified the effects of biosensor concentration on cell edge morphodynamics and on Cdc42 activation location and kinetics, using previously described methods [4,5]. These were unaffected over a specific range of biosensor concentrations, from a low concentration providing the minimal sufficient signal/noise, to a concentration 3 – 15-fold higher. GDI.Cdc42 FLARE (wildtype) biosensor (**a**) and GDI.Cdc42 FLARE (T35S) biosensor (**b**) were expressed in MEFs, and modified meroCBD biosensor (**c**) was microinjected into MEFs expressing the T35S version of the GDI.Cdc42 FLARE biosensor for multiplexed imaging experiments. Each cell analyzed was color-coded based on the intracellular biosensor level. **d,** Scatterplot showing the time lag of the negative peak correlation in individual cells between GDI.Cdc42 FLARE (wildtype) and edge velocity measured in the window band 0.9 – 1.8 μm from the leading edge versus the biosensor expression level. Cells spanning a three-fold difference in expression level are color-coded as in (**a**). Dotted Grey line at –20s indicates the average time lag of the peak correlation at this spatial position (95% confidence interval is [–34s –7s]). **e,** Scatterplot showing the time lag of the negative peak correlation in individual cells between GDI.Cdc42 FLARE (T35S) and edge velocity measured in the window band 0.9 – 1.8 μm from the leading edge versus the biosensor expression level. Cells spanning a 7.5-fold difference in expression level are color-coded as in (**b**)**.** Dotted Grey line at –15.6s indicates the average time lag of the peak cross correlation at this spatial position (95% confidence interval is [–29s –1s]). **f,** Scatterplot showing the time lag of the positive peak correlation in individual cells between Cdc42 activity and edge velocity measured in the window band 0.9 – 1.8 μm from the leading edge versus the concentration of microinjected biosensor. Cells spanning a 15-fold difference in concentration are color-coded as in (**c**). Dotted Grey line at –53s indicates the

average time lag of the peak correlation at this spatial position (95% confidence interval is [–81s –31s]). **g,** Individual cell correlation curves between GDI-Cdc42 complex and edge velocity using the GDI.Cdc42 FLARE (wildtype) biosensor. The expression level of the biosensor in each cell is color-coded as in (**a**). Bootstrap averaged trace of correlation functions is shown in black. The grey dotted line indicates the peak position of the average correlation trace, as in (**d**). **h**, Individual cell cross-correlation curves between GDI-Cdc42 binding and edge velocity using the GDI.Cdc42 FLARE (T35S) biosensor. The expression level of the biosensor in each cell is color-coded as in (**b**). Bootstrap averaged trace of correlation functions is shown in black. The Grey dotted line indicates the peak position of the average correlation trace, as in (**e**). **i**, Individual cell correlation curves between Cdc42 activity and edge velocity using the meroCBD biosensor. The microinjected level of biosensor in each cell is color-coded as in (**c**). Bootstrap averaged trace of correlation functions is shown in black. The Grey dotted line indicates the peak position of the average correlation trace, as in (**f**).

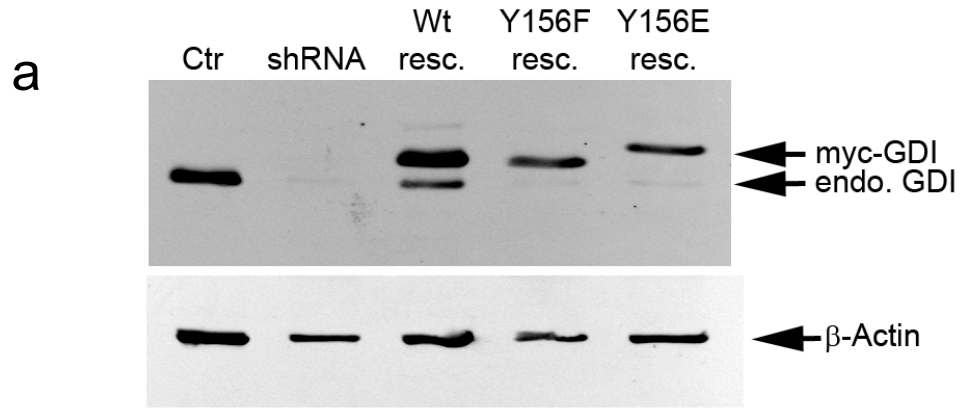

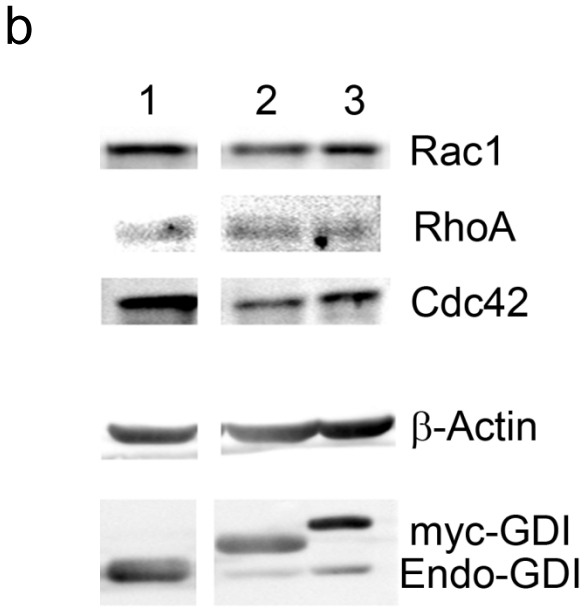

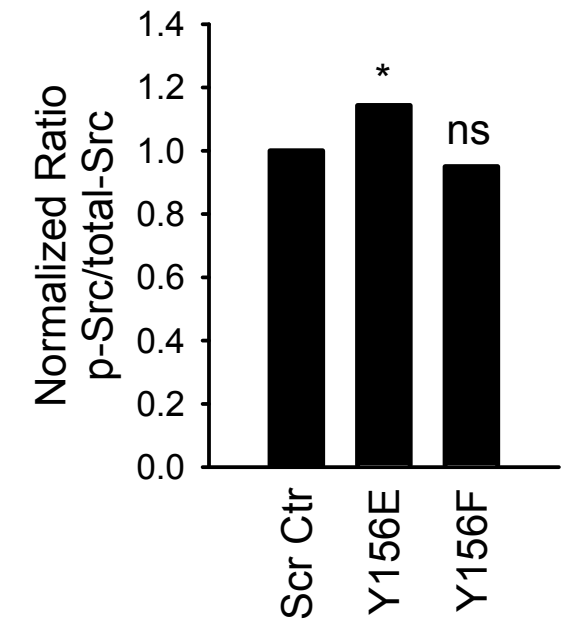

Supplementary Figure 10

Supplementary Fig. 10: Endogenous GDI-depletion and rescue with mutants to address effects of Src-mediated phosphorylation of GDI. a, shRNA against endogenous GDI and the knockdown/rescue of mutant versions of GDI. The knockdown efficiency for endogenous GDI was ~96% at 120 hrs post-transduction. For rescue with wildtype GDI resistant to the shRNA, knockdown was not as efficient (~40%) and led to significant cell death. The uncropped, original blots are shown in **Supplementary Figure 11a**. **b,** Knockdown/rescue using the mutant versions of GDI did not change the expression levels of the Rho family GTPases. Lane 1: Scrambled control RNA; lane 2: KD/rescue with myc-GDI Y156F mutant; lane 3: KD/rescue with myc-GDI Y156E mutant. The uncropped, original blots are shown in **Supplementary Figure 11b**. **c**, Fixed cells were stained for phosphorylated Src (p-Y418) and total Src, and ratio of intensities were determined to reflect the differences in baseline Src activity. * $p = 0.014$, $n = 55 – 69$ cells, pooled from 2 experiments

a

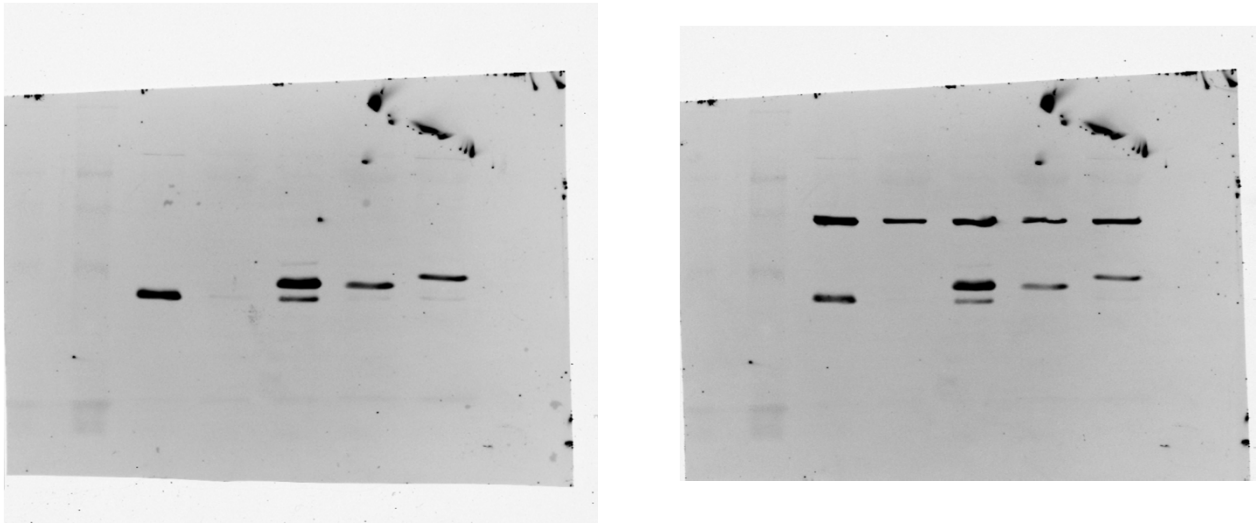

α-GDI + α-β-Actin

b

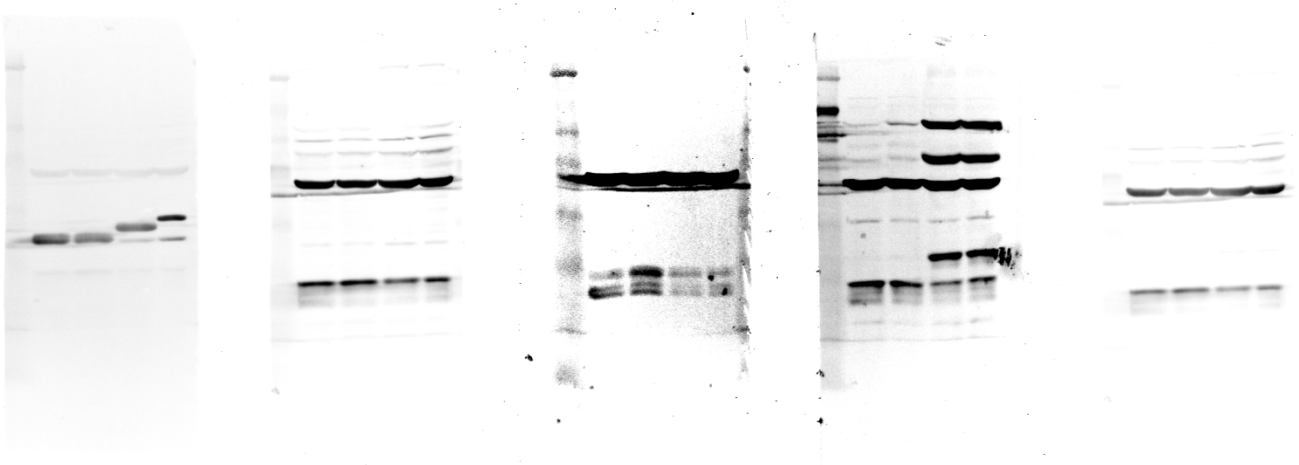

α-GDI α-Rac1 α-RhoA α-Cdc42 α-β-Actin

Supplementary Figure 11

Supplementary Fig. 11: Uncropped Westernblots. a, uncropped, original Westernblots corresponding to **Supplementary Figure 10a**. **b**, uncropped, original Westernblots corresponding to **Supplementary Figure 10b**.

Supplementary Videos

Supplementary Video 1: An example of imaging GDI-Cdc42 binding using the wild-type GDI.Cdc42.FLARE biosensor. Duration of original sequence: 20 min. Magnification 40×, 2×2 binning. Frame interval: 10 sec. Replay: 6 frames/sec. Scale bar: 20 μm.

Supplementary Video 2: An example of imaging GDI-Cdc42 binding using the wild-type GDI.Cdc42.FLARE biosensor. Duration of original sequence: 20 min. Magnification 40×, 2×2 binning. Frame interval: 10 sec. Replay: 6 frames/sec. Scale bar: 20 μm.

Supplementary Video 3: A zoomed example of imaging the GDI-Cdc42 binding using the wild-type GDI.Cdc42.FLARE biosensor. Duration of original sequence: 20 min. Magnification 40×, 2×2 binning. Frame interval: 10 sec. Replay: 6 frames/sec. Scale bar: 10 μm.

Supplementary Video 4: A zoomed example of imaging the GDI-Cdc42 binding using the wild-type GDI.Cdc42.FLARE biosensor. Duration of original sequence: 20 min. Magnification 40×, 2×2 binning. Frame interval: 10 sec. Replay: 6 frames/sec. Scale bar: 10 μm.

Supplementary Video 5: Imaging Cdc42 activity (left) and GDI-Cdc42 binding (T35S mutant version: right) in the same MEF cell. Duration of original sequence: 18 min. Magnification 40×, 2×2 binning. Frame interval: 10 sec. Replay: 6 frames/sec. Scale bar: 20 μm.

Supplementary Video 6: A zoomed example of Cdc42 activity (left) and GDI-Cdc42 binding (T35S mutant version: right) in the same MEF cell. Duration of original sequence: 13 min. Magnification 40×, 2×2 binning. Frame interval: 10 sec. Replay: 6 frames/sec. Scale bar: 10 μm.

Supplementary Video 7: A zoomed example of Cdc42 activity (left) and GDI-Cdc42 binding (T35S mutant version: right) in the same MEF cell. Duration of original sequence: 20 min. Magnification 40×, 2×2 binning. Frame interval: 10 sec. Replay: 6 frames/sec. Scale bar: 10 μm.

Supplementary Video 8: A cell in which GDI has been knocked down and rescued with a Y156F mutant GDI. Cdc42 activity is shown on the left and GDI-Cdc42 binding on the right (T35S mutant version). Duration of original sequence: 20 min. Magnification 40×, 2×2 binning. Frame interval: 10 sec. Replay: 6 frames/sec. Scale bar: 20 μm.

Supplementary Video 9: A zoomed example of a cell where GDI has been knocked down and rescued with a Y156F GDI mutant. Cdc42 activity is shown on the left and GDI-Cdc42 binding on the right (T35S mutant version). Duration of original sequence: 20 min. Magnification 40×, 2×2 binning. Frame interval: 10 sec. Replay: 6 frames/sec. Scale bar: 10 μm.

Supplementary Video 10: A cell in which GDI has been knocked down and rescued with a Y156F mutant GDI. Cdc42 activity is shown on the left and GDI-Cdc42 binding on the right

(T35S mutant version). Duration of original sequence: 13 min. Magnification 40×, 2×2 binning. Frame interval: 10 sec. Replay: 6 frames/sec. Scale bar: 20 μm.

Supplementary Video 11: A zoomed example of a cell where GDI has been knocked down and rescued with a Y156F GDI mutant. Cdc42 activity is shown on the left and GDI-Cdc42 binding on the right (T35S mutant version). Duration of original sequence: 13 min. Magnification 40×, 2×2 binning. Frame interval: 10 sec. Replay: 6 frames/sec. Scale bar: 10 μm.

References

1. Nagai, T., Yamada, S., Tominaga, T., Ichikawa, M. & Miyawaki, A. Expanded dynamic range of fluorescent indicators for Ca(2+) by circularly permuted yellow fluorescent proteins. *Proc Natl Acad Sci U S A* **101**, 10554-9 (2004).
2. Whitlow, M. et al. An improved linker for single-chain Fv with reduced aggregation and enhanced proteolytic stability. *Protein Eng* **6**, 989-95 (1993).
3. Yang, F., Moss, L.G. & Phillips, G.N., Jr. The molecular structure of green fluorescent protein. *Nat Biotechnol* **14**, 1246-51 (1996).
4. Machacek, M. et al. Coordination of Rho GTPase activities during cell protrusion. *Nature* **461**, 99-103 (2009).
5. Machacek, M. & Danuser, G. Morphodynamic Profiling of Protrusion Phenotypes. *Biophys. J.* **90**, 1439-1452 (2006).